GEOPHYSICAL RESEARCH LETTERS, VOL. 36, L02801, DOI:10.1029/2008GL036465, 2009

Integrating anthropogenic heat flux with global climate models

Mark G. Flanner,

Advanced Study Program, National Center for Atmospheric Research

Nearly all energy used for human purposes is dissipated as heat within Earth's land–atmosphere system. Thermal energy released from non-renewable sources is therefore a climate forcing term. Averaged globally, this forcing is only $+0.028\,\mathrm{W\,m^{-2}}$, but over the continental United States and western Europe, it is $+0.39$ and $+0.68\,\mathrm{W\,m^{-2}}$, respectively. Here, present and future global inventories of anthropogenic heat flux (AHF) are developed, and parameterizations derived for seasonal and diurnal flux cycles. Equilibrium climate experiments show statistically-significant continental-scale surface warming ($0.4 - 0.9\,^{\circ}\mathrm{C}$) produced by one 2100 AHF scenario, but not by current or 2040 estimates. However, significant increases in annual-mean temperature and planetary boundary layer (PBL) height occur over gridcells where present-day AHF exceeds $3.0\,\mathrm{W\,m^{-2}}$. PBL expansion leads to a slight, but significant increase in atmospheric residence time of aerosols emitted from large-AHF regions. Hence, AHF may influence regional climate projections and contemporary chemistry-climate studies.

1. Introduction

Heat generated from human energy use has long been recognized as a contributor to the urban heat island. (Other causes include urban differences in albedo, thermal capacity, evapotranspiration, and atmospheric pollutants). Atmospheric effects of large anthropogenic heat flux (AHF) were investigated using an early general circulation model [*Washington*, 1972], and *Chaisson* [2008] recently explored century-scale climate warming that would result from unabated growth in energy use. Although AHF exceeds $100\,\mathrm{W\,m^{-2}}$ in urban centers [*Oke*, 1988; *Ichinose et al.*, 1999] and is treated in some urban- and meso-scale models [e.g., *Kimura and Takahashi*, 1991; *Grimmond and Oke*, 1991; *Fan and Sailor*, 2005; *Dandou et al.*, 2005; *Makar et al.*, 2006], it is neglected in current global climate models (GCMs), likely because its global average is only $\sim$ 1% of greenhouse gas forcing. However, exclusion of present and future AHF may lead to important modeling deficiencies, especially as GCMs continue to resolve finer details, are applied for regional climate projections, and used for studies of chemistry–climate interaction. AHF may significantly alter the evolution of aerosol and gas pollutants because they are typically generated concurrently [*Crutzen*, 2004]. AHF data will also augment studies of urban-global climate interaction, improving as representations of the urban system are coupled with climate models [*Oleson et al.*, 2008b, a]. Here, data and methodology are discussed for incorporating AHF into climate models, and potential impacts on surface temperature, boundary layer height, and aerosol residence time are assessed.

Most energy used for human economy is immediately dissipated as heat, either because of inefficient conversion processes or to serve the purpose of heating. While accomplishing its intended function, some energy is temporarily stored as electrical, mechanical, chemical, or gravitational potential energy, but this component generally transforms to high entropy thermal energy on short timescales (sub-seconds to days). Only a very small portion ($\ll$ 1%) of consumed primary energy converts to radiation that escapes to space without first warming molecules within Earth's atmosphere-land-ocean system. These characteristics of energy flow, consequences of the second law of thermodynamics, enable a simplified approach for translating primary energy consumption into heat flux.

Energy derived from non-renewable sources introduces heat to the Earth System that would not otherwise have been added on relevant timescales, thus constituting a climate forcing. Conversely, energy derived from wind, hydro, and geothermal sources is redistributed kinetic, potential, and thermal energy. This redistribution may also be important for local climate, but is not treated here. Solar energy conversion devices may constitute an anthropogenic forcing because of altered surface albedo (depending also on conversion efficiency), but are also neglected in this study.

2. Methods

Utilizing the second law of thermodynamics, it is assumed that all non-renewable primary energy consumption is dissipated thermally in Earth's atmosphere. Country-specific data of energy consumption from non-renewable sources (coal, petroleum, natural gas, and nuclear) were obtained from the U.S. Energy Information Administration (EIA) (`http://www.eia.doe.gov/emeu/iea`) for year 2005. Fine resolution (2.5×2.5 minute) population density and national boundary data were obtained from Columbia University's Socioeconomic Data and Applications Center (`http://sedac.ciesin.columbia.edu/gpw`). Within each country, total energy consumption was apportioned according to population density (conserving the national total) and converted to annual-mean gridded energy flux. Estimates for 2006–2040 assumed energy-use projections from EIA (high economic growth case) for different regions and economic classifications, listed in Table 1. To explore regional climate impacts of continual exponential growth in energy consumption [*Chaisson*, 2008], an inventory for 2100 was derived assuming uniform $2\,\%\,\mathrm{yr^{-1}}$ growth after 2040. Fine resolution energy flux maps were then re-gridded to the native climate model resolution. An alternative means of distributing country-level energy flux is with night light intensity, which is highly correlated with national energy use, but which can also lead to spurious distributions because of cloudiness and day-length changes [*Makar et al.*, 2006].

To account for temporal variability, the annual-mean anthropogenic heat flux ($\overline{Q_H}$) was scaled with weighting functions dependent on local time of day (t_d) and time of year (t_y):

$$Q_H(t_d, t_y) = \overline{Q_H}\, w_d(t_d)\, w_y(t_y) \qquad (1)$$

Parametric equations for w_d and w_y are based on work from *Sailor and Lu* [2004] and described in Appendix A.

Equilibrium climate simulations were conducted with and without AHF using the National Center for Atmospheric Research (NCAR) Community Atmosphere Model (CAM), version 3.1 [e.g., *Collins et al.*, 2006], coupled to a slab ocean model. Spatial resolution of the simulations was T85, or $\sim 1.4^{\circ} \times 1.4^{\circ}$ near the equator. The spatially- and temporally-varying heat flux was added as dry static energy to the lowest layer of the atmosphere, thus affecting

0094-8276/11/$5.00

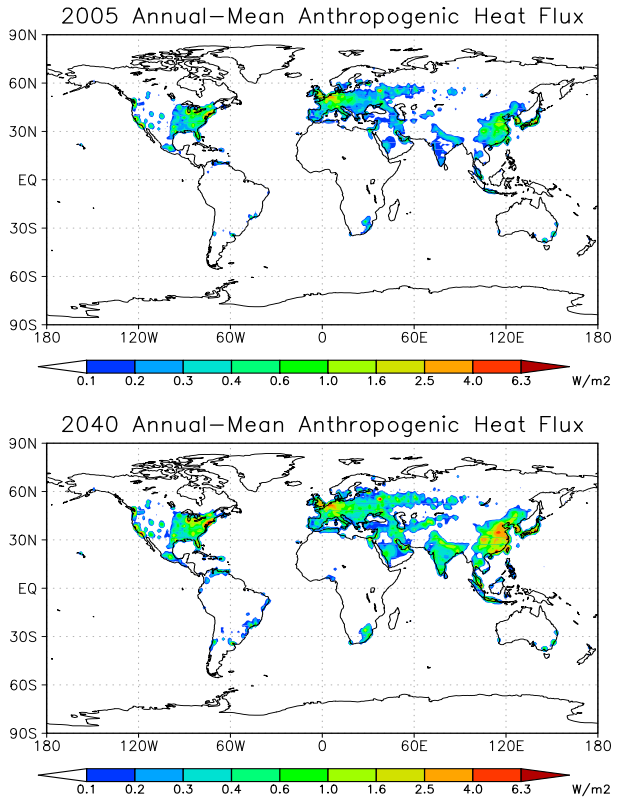

Figure 1. Estimates of annual-mean anthropogenic heat flux resulting from consumption of non-renewable energy sources (coal, petroleum, natural gas, and nuclear) for 2005 (top) and 2040 (bottom). The latter is based on projected growth rates listed in Table 1. The color scale is logarithmic.

temperature, infrared emission, and atmospheric dynamics. The final 20 years of 40-year simulations were analyzed and statistical difference determined with pooled t-tests assuming individual years as realizations. Two 10-year simulations (with and without AHF) were conducted with prognostic, radiatively-passive black carbon aerosol tracers [*Rasch et al.*, 2001] emitted from regions most likely to be influenced by AHF. Emissions of three aerosol tracers were spatially-distributed, from *Bond et al.* [2004], and emissions of one tracer had equal magnitude from all gridcells where $\overline{Q_H}$ exceeded $3\,\mathrm{W\,m^{-2}}$. Global aerosol burdens and atmospheric residence times were analyzed from the final 8 years of these simulations.

Table 1. Projected Non-Renewable Energy Growth Rates Through 2030[a]

Country Classification	Annual Growth Rate (% $\mathrm{yr^{-1}}$)
OECD[b] North America	1.2
OECD Europe	0.8
OECD Asia	1.0
non-OECD Eurasia	1.7
non-OECD Asia	3.6
non-OECD Middle East	2.4
non-OECD Africa	2.5
non-OECD Central and S. America	2.5

[a] Source: EIA International Energy Outlook "High Economic Growth Case," Report #: DOE/EIA-0484(2008)

[b] Organization for Economic Co-operation and Development

3. Results and Discussion

Global distributions of annual-mean AHF for 2005 and 2040 are shown in Figure 1. Global-mean values for these two scenarios are 0.028 and $0.059\,\mathrm{W\,m^{-2}}$. Averaged over the continental United States, western Europe, and China, 2005 fluxes are 0.39, 0.68, and $0.22\,\mathrm{W\,m^{-2}}$, respectively. Applying projected energy growth rates from Table 1, these regional averages increase in 2040 to 0.59, 0.89, and $0.76\,\mathrm{W\,m^{-2}}$. Global-mean AHF in the 2100 scenario is $0.19\,\mathrm{W\,m^{-2}}$. The greatest 2005 gridcell flux at T85 model resolution is $8.1\,\mathrm{W\,m^{-2}}$ (Tokyo), and is $48\,\mathrm{W\,m^{-2}}$ (New York) at $0.5^\circ \times 0.5^\circ$ resolution. Gridded 2005–2040 AHF data (0.5° resolution) are available at: `http://www.cgd.ucar.edu/tss/ahf`.

Diurnal and seasonal distributions of AHF are shown in Figure 2. Parameterizations of these cycles (Appendix A) are derived from figures in *Sailor and Lu* [2004]. The diurnal heat flux cycles from U.S. cities examined in this study show similar features, generally characterized by a sharp morning spike, local maxima during morning and evening traffic hours, and a slow reduction during night. *Sailor and Lu* [2004] also show greater energy expenditures during winter in higher-latitude cities, associated with heating, which is accounted for with a latitudinally-dependent sinusoidal function (Appendix A.). These parameterizations provide a framework for climate model application, but are not universal descriptors of heat flux variability. For example, seasonal variability of rural energy use depends on agricultural and precipitation cycles. Amplified summer energy consumption associated with air conditioning varies with climate and economic development, and diurnal variability in regions with high-intensity industry is damped because of continual peak-load operation. Equations in Appendix A include several tunable parameters that control different components of these cycles, described in Table A1, offering the flexibility of improving spatial/temporal variability of AHF in future studies. An alternative method for incorporating AHF, more

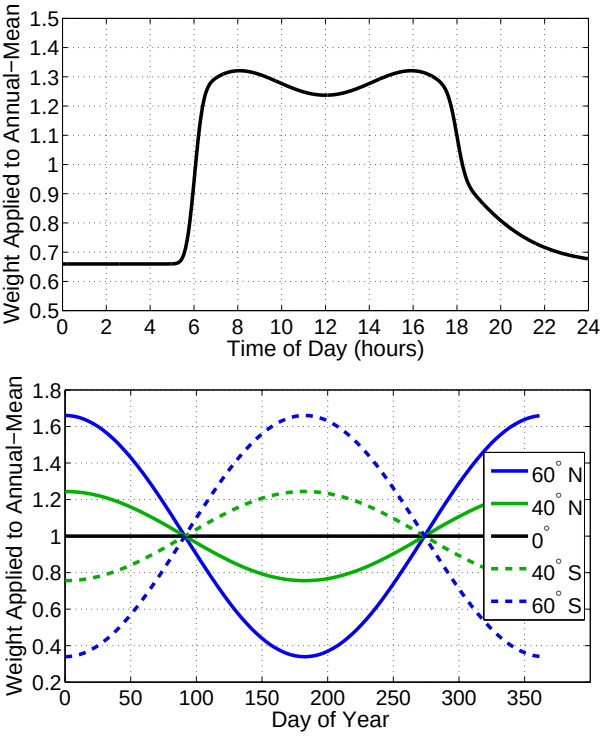

Figure 2. Diurnal (top) and seasonal (bottom) cycles of anthropogenic heat flux based on *Sailor and Lu* [2004], applied as weights to the annual-mean flux. Parametric equations for these functions are described in Appendix A.

Table 2. Statistically Significant Equilibrium Climate Changes[a]

	Continental United States	Europe	East Asia	Gridcells with $\overline{Q_H} > 3.0\,\mathrm{W\,m^{-2}}$
2005 Annual-mean T_s (°C)	–	–	–	$+0.15$ $(n = 14)$
2005 Annual-mean h_{pbl} (m)	$+16$	–	–	$+32$
2040 Annual-mean T_s (°C)	–	–	–	$+0.24$ $(n = 60)$
2040 Annual-mean h_{pbl} (m)	–	–	–	$+29$
Aerosol residence time	–	–	–	$+2.5\%$
2100 Annual-mean T_s (°C)	$+0.44$	$+0.54$	$+0.88$	$+0.76$ $(n = 414)$
2100 Annual-mean h_{pbl} (m)	$+15$	$+21$	$+45$	$+53$

[a] Changes significantly different from zero at the 0.05 level
T_s: 2-meter air temperature
h_{pbl}: Planetary boundary layer height

compatible with an Earth System Modeling framework, is to interactively prognose heat flux based on local temperature and assumptions about heating/cooling practices [*Sailor and Vasireddy*, 2006; *Oleson et al.*, 2008a]. This approach captures important feedback, such as increased air conditioning needs caused by heat generated from cooling units. Such prognostic AHF schemes should, however, be constrained with data such as that presented here.

Regionally-averaged heat fluxes are sufficiently large ($\sim 1\,\mathrm{W\,m^{-2}}$) to investigate whether they have a significant effect on large-scale climate variables, such as temperature and planetary boundary layer (PBL) height. To explore this, equilibrium states from simulations with and without 2005, 2040, and 2100 AHF are compared over regions with large heat flux: the Continental United States ($30-45$°N, $235-290$°E), Europe ($40-60$°N, $350-40$°E), and East Asia ($23-42$°N, $100-130$°E). Annual-mean temperature and PBL height changes (averaged only over land) are listed in Table 2. These results show regionally-averaged changes for 2005 and 2040 that are mostly small and not significant at the 0.05 level, suggesting that current and near-future AHF does not have much influence on continental-scale temperature. Contemplating beyond 2040, however, *Chaisson* [2008] argues that 3°C global warming could result within 300 years from AHF alone, if non-renewable energy consumption continues to grow at $2\,\%\,\mathrm{yr^{-1}}$. Although future energy practices are highly uncertain, sources that could sustain such growth while constituting a climate forcing include nuclear fusion and those that increase total solar energy absorbed by Earth. The 2100 AHF scenario produces substantial warming ($0.4-0.9\,^{\circ}\mathrm{C}$) and elevated PBL height ($15-45\,\mathrm{m}$) over large regions (Table 2).

Although near-future regional climate changes are not significant, annual-mean temperature change over gridcells subject to more than $3.0\,\mathrm{W\,m^{-2}}$ heat flux is significant in both 2005 ($+0.15$°C) and 2040 ($+0.24$°C) experiments. Thus, there is a noticeable, but locally-constrained urban heat island signal in global simulations with present-day AHF. Although the affected area is small, 9% of the world population inhabits area where $\overline{Q_H} > 3.0\,\mathrm{W\,m^{-2}}$ (at $0.5^{\circ} \times 0.5^{\circ}$ resolution), and this proportion will likely be much greater in 2040 as per-capita energy consumption rises and populations urbanize. Moreover, total area subject to $\overline{Q_H} > 3.0\,\mathrm{W\,m^{-2}}$ is resolution-dependent, increasing from $2.3 \times 10^5\,\mathrm{km^2}$ at T85 resolution to $4.7 \times 10^5\,\mathrm{km^2}$ at 0.5° resolution.

Heat flux is expected to have the greatest surface temperature influence during nocturnal winter, because of stable boundary layers in cold regions, greater fractional contribution of AHF to the surface energy energy budget [e.g., *Fan and Sailor*, 2005], and greater energy consumption during winter at higher latitudes (Figure 2). Interestingly, nocturnal winter (December–February) warming over high-AHF gridcells is generally less than annual-mean warming, while PBL expansion is greater (not shown). PBL expansion acts as a negative feedback on surface temperature change by increasing the mass of well-mixed air in (near) thermal equilibrium with the heat source. Nonetheless, these simulations do not show the enhanced winter night warming from AHF demonstrated in meso-scale studies [*Fan and Sailor*, 2005; *Dandou et al.*, 2005], perhaps because of smaller gridcell heat flux (from coarser model resolution) and reduced night flux (Figure 2). Also, amplified nocturnal warming is sensitive to boundary layer parameterization [*Fan and Sailor*, 2005]. Simulated temperature effects from AHF will also depend on representation of the urban system [e.g., *Masson*, 2000; *Best*, 2005; *Oleson et al.*, 2008b]. Additional heat capacity of buildings, for example, damps diurnal temperature extremes.

Finally, aerosols and gases emitted from regions with elevated PBL height may be lofted higher in the atmosphere, influencing species residence time and radiative forcing. Mean residence times of four passive aerosol tracers are compared with and without 2040 AHF influence (Table 2). Current fossil fuel and biofuel sources of black carbon emitted from the U.S., Europe, and East Asia do not have statistically different atmospheric residence times. Aerosols emitted only from regions with $\overline{Q_H} > 3.0\,\mathrm{W\,m^{-2}}$, however, reside 2.5% longer in the atmosphere (significant at 0.01). As atmospheric burden scales with residence time, radiative forcing of these aerosols would increase about (or slightly less than) proportionately. Currently, only about 4% of fossil fuel black carbon is emitted from T85 gridcells with $\overline{Q_H} > 3.0\,\mathrm{W\,m^{-2}}$. However, this fraction rises to 14% when assuming 2040 AHF estimates. On finer spatial scales, the proportion of emissions coinciding with large heat sources is certainly much greater. Indeed, black carbon and many other pollutants are only generated from high-temperature combustion. However, the influence of micro-scale heating on pollutant residence time remains unknown.

4. Conclusions

Anthropogenic heat flux (AHF), a consequence of non-renewable energy use and the second law of thermodynamics, is not included in state-of-the-art climate simulations. Here, global inventories and parameterizations of AHF, suitable for climate model application, are developed for 2005–2100. Although global-mean AHF is small, it may approach $1\,\mathrm{W\,m^{-2}}$ over large regions by 2040. Climate simulations do not show significant continental-scale surface temperature response to this forcing in the near-future, but annual-mean warming of $0.4-0.9\,^{\circ}\mathrm{C}$ occurs over large industrialized regions in one 2100 scenario, supporting recent work by *Chaisson* [2008]. In present-day experiments, gridcells subject to AHF greater than $3.0\,\mathrm{W\,m^{-2}}$ experience significant warming and elevated planetary boundary layers, causing aerosols emitted from these areas to reside slightly longer in the atmosphere. On finer spatial scales, resolved AHF becomes larger and coincides more closely with industrial pollutant emissions and human population. Thus, as Earth System Models incorporate more sophisticated representations of the urban system and are applied to understand linkages between pollutants, climate, and human health, inclusion of AHF will become more important. Data presented here may also help constrain prognostic AHF schemes.

Appendix A: Equations for diurnal and seasonal AHF cycles

The diurnal weighting function w_d depends on fractional time of day t_d as:

$$w_d(t_d) = N(t_d)\, E1\, b_1 + H(t_d)\, E1\, E2 + b_2 \quad \text{(A1)}$$

where $N(t_d)$ is the normal distribution:

$$N(t_d) = \frac{1}{\sigma\sqrt{2\pi}}\, \mathrm{e}^{-(t_d-\mu)^2/2\,\sigma^2} \quad \text{(A2)}$$

$H(t_d)$ is the harmonic function:

$$H(t_d) = A_1\, \cos(2\pi\, f\, t_d) \quad \text{(A3)}$$

and E1 and E2 are error functions:

$$E1 = 0.5\, \{\mathrm{erf}[\alpha(t_d - \mu + \epsilon)/\sigma] + 1.0\} \quad \text{(A4)}$$

$$E2 = 0.5\, \{\mathrm{erf}[-\alpha(t_d - \mu - \epsilon)/\sigma] + 1.0\} \quad \text{(A5)}$$

Values applied for all parameters are listed in Table A1, which also describes features of the diurnal cycle controlled by each parameter. Future model implementations may prescribe spatially-varying parameters to account for variability in (e.g.,) traffic, nighttime heating, and commercial energy use.

The seasonal weighting function w_y depends on fractional time of year t_y as:

$$w_y(t_y) = 1 + A_2(\theta)\, \sin[2\pi(t_y + 0.25)] \quad \text{(A6)}$$

where θ is latitude in degrees. The latitudinally-dependent amplitude is:

$$\begin{aligned} A_2(\theta) &= 1 - \mathrm{e}^{-(\theta-33)/25} && \text{for } \theta > 33 \\ A_2(\theta) &= 0 && \text{for } -33 \le \theta \le 33 \\ A_2(\theta) &= -(1 - \mathrm{e}^{(\theta+33)/25}) && \text{for } \theta < -33 \end{aligned} \quad \text{(A7)}$$

Thus, no seasonal cycle is applied to regions equator-ward of 33°. Both weighting functions are normalized to have mean equal to 1, conserving the annual-mean flux.

Acknowledgments. I thank Dave Lawrence, Sam Levis, Keith Oleson, and two anonymous reviewers for providing instructive comments on this paper, and Imran Sheikh and Ben Sanderson for enlightening conversations. The National Center for Atmospheric Research (NCAR) is sponsored by the National Science Foundation. Computations supported by NCAR facilities and NSF ATM-0321380. Research also supported by NSF-0758369.

References

Best, M. J. (2005), Representing urban areas within operational numerical weather prediction models, *Boundary-Layer Meteorology*, *114*, 91–109.

Bond, T. C., D. G. Streets, K. F. Yarber, S. M. Nelson, J.-H. Woo, and Z. Klimont (2004), A technology-based global inventory of black and organic carbon emissions from combustion, *J. Geophys. Res.*, *109*, D14203, doi:10.1029/2003JD003697.

Chaisson, E. J. (2008), Long-term global heating from energy use, *EOS Transactions*, *89*(28), 253–254.

Collins, W. D., et al. (2006), The Community Climate System Model Version 3 (CCSM3), *J. Climate*, *19*, 2122–2161.

Crutzen, P. J. (2004), New directions: The growing urban heat and pollution "island" effect - impact on chemistry and climate, *Atmos. Environ.*, *38*, 3539–3540.

Dandou, A., M. Tombrou, E. Akylas, N. Soulakellis, and E. Bossioli (2005), Development and evaluation of an urban parameterization scheme in the Penn State/NCAR Mesoscale Model (MM5), *J. Geophys. Res.*, *110*, D10102.

Fan, H., and D. J. Sailor (2005), Modeling the impacts of anthropogenic heating on the urban climate of Philadelphia: a comparison of implementations in two PBL schemes, *Atmos. Environ.*, *39*, 73–84.

Grimmond, C. S. B., and T. R. Oke (1991), An evapotranspiration-interception model for urban areas, *Water Resour. Res.*, *27*, 1739–1755.

Ichinose, T., K. Shimodozono, and K. Hanaki (1999), Impact of anthropogenic heat on urban climate in Tokyo, *Atmos. Environ.*, *33*, 3897–3909.

Kimura, F., and S. Takahashi (1991), The effects of land-use and anthropogenic heating on the surface temperature in the Tokyo metropolitan area: a numerical experiment, *Atmos. Environ. B*, *25*, 155–164.

Makar, P. A., S. Gravel, V. Chirkov, K. B. Strawbridge, F. Froude, J. Arnold, and J. Brook (2006), Heat flux, urban properties, and regional weather, *Atmos. Environ.*, *40*, 2750–2766.

Masson, V. (2000), A physically-based scheme for the urban energy budget in atmospheric models, *Boundary-Layer Meteorology*, *94*, 357–397.

Oke, T. R. (1988), The urban energy balance, *Progress in Physical Geography*, *12*, 471–508.

Oleson, K. W., G. B. Bonan, J. Feddema, and M. Vertenstein (2008a), An urban parameterization for a global climate model. Part II: Sensitivity to input parameters and the simulated urban heat island in offline simulations, *J. Appl. Meteor. and Climatology*, *47*, 1061–1076.

Oleson, K. W., G. B. Bonan, J. Feddema, M. Vertenstein, and C. S. B. Grimmond (2008b), An urban parameterization for a global climate model. Part I: Formulation and evaluation of two cities, *J. Appl. Meteor. and Climatology*, *47*, 1038–1060.

Rasch, P. J., W. D. Collins, and B. E. Eaton (2001), Understanding the Indian Ocean Experiment (INDOEX) aerosol distributions with an aerosol assimilation, *J. Geophys. Res.*, *106*(D7), 7337–7355.

Sailor, D. J., and L. Lu (2004), A top-down methodology for developing diurnal and seasonal anthropogenic heating profiles for urban areas, *Atmos. Environ.*, *38*, 2737–2748.

Sailor, D. J., and C. Vasireddy (2006), Correcting aggregate energy consumption data to account for variability in local weather, *Environmental Modelling and Software*, *21*, 733–738.

Washington, W. M. (1972), Numerical climatic-change experiments: The effect of man's production of thermal energy, *J. Appl. Meteor.*, *11*, 768.

M. G. Flanner, National Center for Atmospheric Research, P.O. Box 3000, Boulder CO 80307. (mflanner@ucar.edu)

Table 3. (Table A1 in Appendix A): Diurnal Cycle Parameters

Parameter	Value	Feature Controlled
b_1	0.451	Daytime amplification
b_2	0.8	Daytime amplification
σ	0.18	Slope of evening tapering
μ	0.5	Timing of morning and evening ramps
A_1	-0.3	Amplitude of morning and evening traffic maxima
f	2.0	Timing of morning and evening traffic maxima
α	10.0	Slope of morning increase
ϵ	0.25	Timing of morning and evening ramps